Analysis of the Acceleration Characteristics of Non-Redundant Manipulators

Alan Bowling and Oussama Khatib

Robotics Laboratory
Computer Science Department
Stanford University
Stanford, CA, USA 94305

Abstract

The study of the acceleration properties at the end effector is important in the analysis, design, and control of robot manipulators. In previous efforts aimed at addressing this problem, the end-effector acceleration has been treated as a vector combining both the linear and angular accelerations. The methodology presented in this article provides characterizations of these two different types of accelerations and describes the relationship between them. This work is an extension of our previous studies on manipulator inertial and acceleration properties. The treatment relies on the ellipsoid expansion *model, a simple geometric approach to efficiently analyze end-effector accelerations. Results of the application of this analysis to the PUMA 560 manipulator are discussed.*

1 Introduction

The end-effector acceleration properties are important performance indicators for manipulator systems. Several methods have been proposed for the analysis of end-effector accelerations resulting in different measures of acceleration characteristics. One such measure is the isotropic acceleration: the amount of acceleration achievable in or about every direction.

When determining this measure for systems with many degree of freedom (DOF) it is necessary to account for linear as well as angular accelerations. The non-homogeneity between linear and angular accelerations has been often ignored and these two quantities have been treated as component of a single vector.

Yoshikawa [1] proposed the Dynamic Manipulability Ellipsoid (DME). Here linear and angular accelerations are analyzed as components of a single vector. Scaling factors are used to bring the differing magnitudes into range with each other. In practice these scaling factors are difficult to determine for many DOF systems and their selection is somewhat arbitrary. In addition, the method yields a conservative estimate of the isotropic acceleration.

In an earlier study, we have proposed [2] the hyper-parallelepiped of acceleration as a description of end-effector accelerations. The exact isotropic acceleration can be found by inscribing a hyper-sphere within the acceleration hyper-parallelepiped. However, this process proves difficult when analyzing systems with many DOF. In addition, linear and angular accelerations have been also treated as components of the same vector and weighting factors have been used to deal with their different nature.

The work presented in this article is a pursuit of the previous study with the aim of explicitly addressing the differences between linear and angular acceleration. This work has resulted in the *ellipsoid expansion* approach. In this approach linear and angular accelerations are considered as two separate entities.

The ellipsoid expansion method provides a simple geometric solution to the system of inequalities associated with the bounds on actuator torques. It allows an exact determination of the isotropic linear acceleration, the angular acceleration, and the relationship between them. The results of the application of this approach to the PUMA 560 manipulator are presented.

2 Torque/Acceleration Relationship

In this section the model which is the basis for the *ellipsoid expansion* model is derived. The derivation

0-8186-7108-4/95 $4.00

begins with the operational space equations of motion,

$$\Lambda(\mathbf{q})\dot{\vartheta} + \mu(\mathbf{q}, \dot{\mathbf{q}}) + \mathbf{p}(\mathbf{q}) = \mathbf{F} \tag{1}$$

where

$$\vartheta \triangleq \begin{bmatrix} \mathbf{v} \\ \omega \end{bmatrix} = J_0(\mathbf{q})\dot{\mathbf{q}}. \tag{2}$$

In equation (1) $\mathbf{q}$ is the vector of n joint coordinates, $\Lambda(\mathbf{q})$ is the psuedo-kinetic matrix or mass matrix, $\mu(\mathbf{q}, \dot{\mathbf{q}})$ is the centrifugal and Coriolis force vector, $\mathbf{p}(\mathbf{q})$ is the gravity force vector, and $\mathbf{F}$ is the vector of forces applied at the end-effector. In equation (2) $\mathbf{v}$ and ω are the end-effector linear and angular velocities and $J_0(\mathbf{q})$ is the basic Jacobian matrix, (for notational simplicity $(\mathbf{q})$ and $(\mathbf{q}, \dot{\mathbf{q}})$ will be omitted from subsequent equations).

Using the relationship between τ, the vector of joint torques, and $\mathbf{F}$,

$$\tau = J_0^T \mathbf{F} \tag{3}$$

in equation (1) yields,

$$J_0^T(\Lambda\dot{\vartheta} + \mu + \mathbf{p}) = \tau. \tag{4}$$

The bounds on τ can be written as

$$-\tau_{bound} \leq \tau \leq \tau_{bound}. \tag{5}$$

To normalize the bounds on τ, we introduce the diagonal matrix N with components $N_{ii} = \frac{1}{\tau_{bound(i)}}$. Now using equations (4) and (5) yields,

$$-\mathbf{1} \leq NJ_0^T(\Lambda\dot{\vartheta} + \mu + \mathbf{p}) \leq \mathbf{1}; \tag{6}$$

where $\mathbf{1}$ is a vector of length n with each element equal to one. Using equation (2) the above equation can be rewritten as,

$$\tau_{lower} \leq [E_{\mathbf{v}}\ E_{\omega}] \begin{bmatrix} \dot{\mathbf{v}} \\ \dot{\omega} \end{bmatrix} + \begin{bmatrix} \vartheta^T M_1 \vartheta \\ \vdots \\ \vartheta^T M_n \vartheta \end{bmatrix} \leq \tau_{upper}; \tag{7}$$

where M_i are symmetric matrices and,

$$[E_{\mathbf{v}}\ E_{\omega}] = NJ_0^T\Lambda; \tag{8}$$

$$\begin{bmatrix} \vartheta^T M_1 \vartheta \\ \vdots \\ \vartheta^T M_n \vartheta \end{bmatrix} = NJ_0^T\mu; \tag{9}$$

$$\tau_{upper} = \mathbf{1} - NJ_0^T\mathbf{p}; \tag{10}$$

$$\tau_{lower} = -\mathbf{1} - NJ_0^T\mathbf{p}. \tag{11}$$

Finally, the governing equation for this analysis is

$$\boxed{\tau_{lower} \leq E_{\mathbf{v}}\dot{\mathbf{v}} + E_{\omega}\dot{\omega} + \begin{bmatrix} \vartheta^T M_1 \vartheta \\ \vdots \\ \vartheta^T M_n \vartheta \end{bmatrix} \leq \tau_{upper}} \tag{12}$$

The separation of linear and angular accelerations in equation (12) is motivated by the need to analyze each of them independently. The Coriolis/centrifugal terms can also be analyzed to determine the general effect end-effector velocities have on the isotropic accelerations.

3 Ellipsoid Expansion Model

3.1 Overview

The basic approach used to analyze equation (12) is to visualize each component of the equation as a geometric object. This allows a simple determination of the relationships between each component of the equation. This approach differs from other studies essentially in that quantities of interest are mapped from acceleration space into torque space; other approaches do the opposite. A significant advantage of this approach is that the torque bounds can be represented and used in their simplest form, a hypercube.

The visualization process begins by considering the bounds of a simple vector inequality;

$$\tau_{lower} \leq \dot{\mathbf{v}} \leq \tau_{upper}. \tag{13}$$

The bounds are represented as an n-dimensional hypercube whose center is shifted from the origin by the gravity effect, i.e. $NJ_0^T\mathbf{p}$. Any vector $\dot{\mathbf{v}}$ which lies within this hypercube satisfies the above inequality. When considering isotropic acceleration we are concerned with $\dot{\mathbf{v}}$ having the largest possible magnitude in all directions. This is represented by a hyper-sphere with some radius a,

$$\dot{\mathbf{v}}^T\dot{\mathbf{v}} = a^2. \tag{14}$$

The value of a at which the hyper-sphere is tangent to one of faces of the bounding hypercube yields the largest possible acceleration achievable in every direction. a is determined by starting with the unit hyper-sphere, $a = 1$, and expanding/contracting it, increasing/decreasing a, until the first bound is touched as illustrated in Figure 1.

In practice, since there are $2n$ faces on the bounding hypercube, it is necessary to examine only $2n$ points on the hyper-sphere to determine which one touches a boundary first. Since we are working with a hyper-sphere, or later a hyper-ellipsoid, these $2n$ points are

easy to determine. In the following sections this process will be used to analyze each of the terms within the inequality of equation (12).

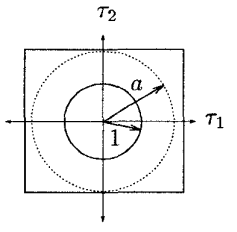

Figure 1: Isotropic Linear Acceleration.

3.2 Acceleration Terms

Consider the case where $\dot{\omega} = \dot{\mathbf{q}} = 0$. Equation (12) becomes,

$$\tau_{lower} \leq E_{\mathbf{v}}\dot{\mathbf{v}} \leq \tau_{upper}. \tag{15}$$

The effect of the matrix $E_{\mathbf{v}}$ on the isotropic acceleration surface, (14), can be determined using the relationship between acceleration and torque;

$$\tau_{\mathbf{v}} = E_{\mathbf{v}}\dot{\mathbf{v}}.$$

With respect to $\dot{\mathbf{v}}$, the above relationship represents an over constrained system of equations, whose unique solution is given by

$$\dot{\mathbf{v}} = E_{\mathbf{v}}^{+}\ \tau_{\mathbf{v}}; \tag{16}$$

where $E_{\mathbf{v}}^{+}$ is the left inverse of $E_{\mathbf{v}}$, (given by the left pseudo-inverse $E_{\mathbf{v}}^{+} = (E_{\mathbf{v}}^T\ E_{\mathbf{v}})^{-1}\ E_{\mathbf{v}}^T$). Using equation (16), the sphere of acceleration $\dot{\mathbf{v}}^T\dot{\mathbf{v}} = a^2$ is transformed into,

$$\tau_{\mathbf{v}}^T(E_{\mathbf{v}}E_{\mathbf{v}}^T)^{+}\tau_{\mathbf{v}} = a^2. \tag{17}$$

Since $E_{\mathbf{v}}$ is at most of rank three, this surface is a hyper-cylinder in n-dimensions. However, we may eliminate the cylindrical portion of this surface because only torques which contribute solely to end-effector linear acceleration are considered. This corresponds to excluding vectors in the null space of $E_{\mathbf{v}}^{+}$. The remaining surface is an hyper-ellipsoid in, at most, a three dimensional subspace.

The isotropic acceleration is determined by expanding/contracting the ellipsoid (17), changing a, until it lies within and is tangent to the torque bounds. In Figure 2 this process is shown for a simple case and Figure 3 shows a more general case. The dashed ellipse in both figures corresponds to $a = 1$. Note that only the vectors associated with the tangent points, $2n$ points, need to be examined.

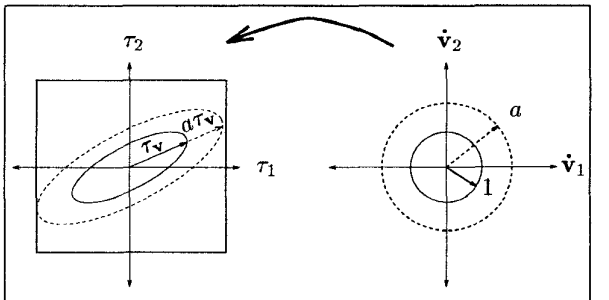

Figure 2: Ellipse $\tau_{\mathbf{v}}$.

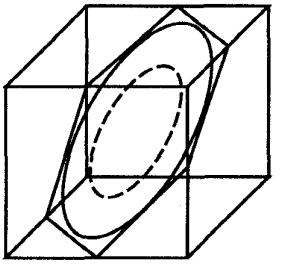

Figure 3: Ellipsoid in 3D.

Let us now consider the case where $\dot{\mathbf{q}} = 0$;

$$\tau_{lower} \leq E_{\mathbf{v}}\dot{\mathbf{v}} + E_{\omega}\dot{\omega} \leq \tau_{upper}.$$

Just as in the linear case, the isotropic angular acceleration is represented as a sphere with some radius b,

$$\dot{\omega}^T\dot{\omega} = b^2.$$

This sphere is mapped into torque space using the relationship

$$\tau_{\omega} = E_{\omega}\dot{\omega}$$

resulting in a second ellipsoid,

$$\tau_{\mathbf{v}}^T(E_{\mathbf{v}}E_{\mathbf{v}}^T)^{+}\tau_{\mathbf{v}} = a^2 \quad \text{and} \quad \tau_{\omega}^T(E_{\omega}E_{\omega}^T)^{+}\tau_{\omega} = b^2. \tag{18}$$

To insure that the sum of $a\tau_{\mathbf{v}}$ and $b\tau_{\omega}$ remains within the bounds, all possible combinations of these two vectors must be considered. This process is represented as a mapping of one ellipsoid onto every point on the surface of the other ellipsoid, graphically illustrated in Figure 4. As before it is only necessary to examine the vectors representing the tangency points between the resulting surface and the bounding box. These points are found by adding vectors representing the tangency point on each surface corresponding

to the same boundary as illustrated Figure 5.

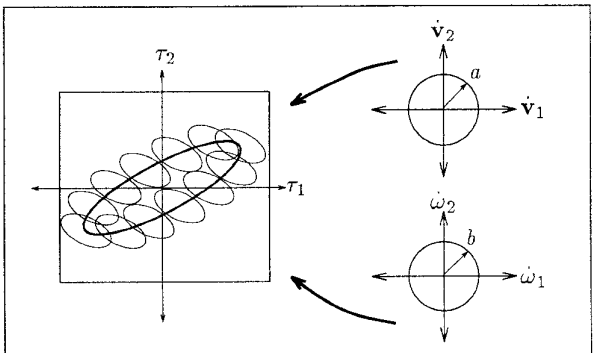

Figure 4: Ellipsoids Added.

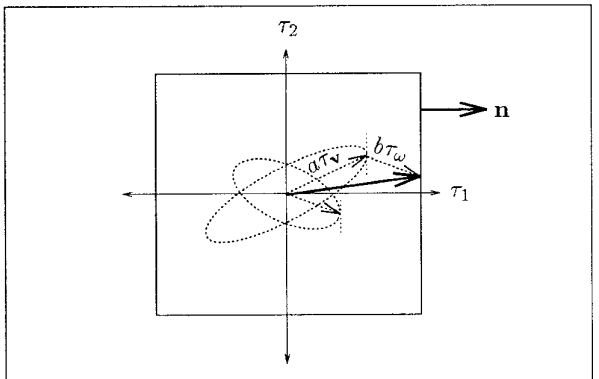

Figure 5: Tangency Point.

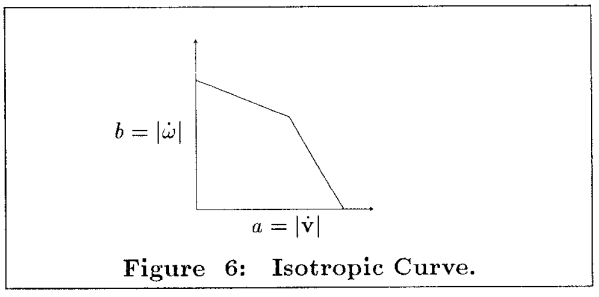

Figure 6: Isotropic Curve.

The possible combinations of $a\tau_{\mathbf{v}}$ and $b\tau_{\omega}$ yielding a resultant which touches a bound is described by the following equation;

$$\mathbf{n}_i \cdot (a\tau_{\mathbf{v}_i} + b\tau_{\omega_i}) = \tau_{upper_i} \text{ or } \tau_{lower_i} \qquad (19)$$

where n_i is the vector normal to the boundary plane i as shown Figure 5. $2n$ of these relationships are found for the $2n$ boundaries. The equation from this set which yields the smallest value for a given b or vice versa determines a curve which is piecewise linear as illustrated in Figure 6. A discontinuity in the curve occurs when the limiting boundary changes.

3.3 Centrifugal and Coriolis Forces

Another aspect of the analysis involves determining the effect of end-effector velocities on the isotropic accelerations. A specific velocity is analyzed as a boundary shift, just as the gravity terms were. For a more general characterization, surfaces representing all possible velocities, $\mathbf{v}^T\mathbf{v} = c^2$ and $\omega^T\omega = d^2$, can be mapped through the Coriolis/centrifugal coefficient matrices yielding a hypothetical surface. However, determining an analytic expression for such a surface is quite difficult. This problem, which is currently under investigation, will not be discussed here.

To integrate the effect of these forces, we resort to the use of scaling factors between linear and angular velocities. Clearly, this is not an ideal solution, as discussed in Section 1, but it does yield useful information.

$$\vartheta^T W \vartheta = e^2 \qquad (20)$$

where W is an invertible diagonal positive definite matrix. A reasonable scaling factor can be found in the a-b isotropicity curve as the slope of one of the line segments. A change of variables, $\mathbf{y} = W^{1/2}\vartheta$ yields,

$$\mathbf{y}^T\mathbf{y} = e^2 \quad \text{and} \quad \tau_c = \begin{bmatrix} \mathbf{y}^T(W^{-1/2})^T M_1 W^{-1/2}\mathbf{y} \\ \vdots \\ \mathbf{y}^T(W^{-1/2})^T M_n W^{-1/2}\mathbf{y} \end{bmatrix} \qquad (21)$$

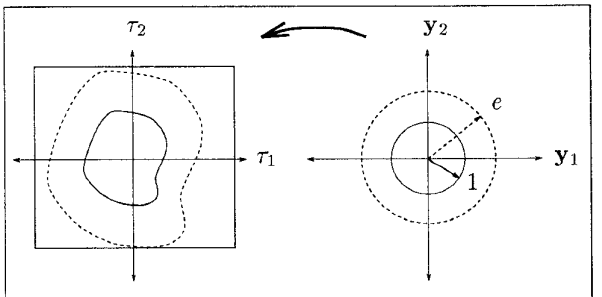

Figure 7: Centrifugal/Coriolis Surface.

This mapping produces a surface in torque space as shown Figure 7. The vectors of the resulting surface representing the tangency point to a particular boundary has the largest component in the direction of the vector normal to that boundary plane as illustrated Figure 8. By analyzing each component of the centrifugal/Coriolis vector, we can easily determine the vectors $\mathbf{y}$ which yield the largest (most positive) and

the smallest (most negative) values for that component.

These vectors are then added to the corresponding acceleration torque vectors yielding a relationship between the three magnitudes;

$$\mathbf{n}_i \cdot (a\tau_{\mathbf{v}_i} + b\tau_{\omega_i} + e\tau_{c_i}) = \tau_{upper_i} \text{ or } \tau_{lower_i}. \quad (22)$$

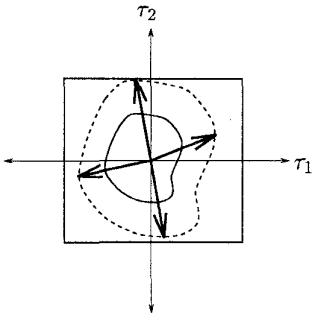

Figure 8: Tangents.

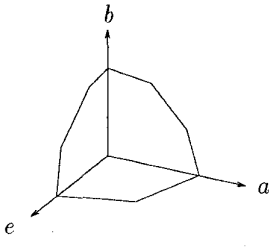

Figure 9: Isotropic Surface.

The representation of this information is a three-dimensional surface with planar facets. In Figure 9 only the intersection of the surface with the three coordinate planes is shown because most of the interesting information lies in these planes. In the *a*-*b* plane the information shown in Figure 6 is duplicated. Consider the point along the e axis where a and b are driven to zero. This point gives the state of end-effector velocity when, in some direction, all actuator torque is being used to compensate for Coriolis/centrifugal and gravity forces. Given that the velocity must lie on the surface $\vartheta^T W \vartheta = e^2$, this point represents a velocity condition at which the manipulator will not be able to accelerate in some direction.

3.4 Additional Characteristics

The previous analysis relies on finding the face of the hypercube boundary which is touched first by the ellipsoids. Knowing which boundary is touched first, the limiting actuator(s), is quite useful in analyzing and choosing actuator capacity. Depending on the manipulator, increasing the most limiting actuator torque(s) may increase the isotropic accelerations.

The proposed model also yields useful information concerning the variance of achievable end-effector accelerations in different directions, at a given configuration. This information is simply given by the condition numbers of the matrices $E_{\mathbf{v}}$ and E_ω, $\kappa(E_{\mathbf{v}})$ and $\kappa(E_\omega)$.

4 Application: PUMA 560

The approach presented above is illustrated here on the PUMA 560. The motor torque bounds are found by subtracting the breakaway torques from the maximum torques as given in [3];

$$\tau_{bound} = \{1.45, 1.70, 1.62, 0.30, 0.27, 0.26\} Nm.$$

Figures 10 through 13 show the results of analysis of the PUMA 560 for different manipulator parameters. For all cases the weighting matrix, W, is identity. In each figure the label beside each line segment indicates the limiting actuator for that segment. Many comparisons can be made between these figures but only a few of these will be discussed below.

In Figure 10 isotropicity information for the wrist point of the PUMA 560 at a well conditioned configuration in the workspace is shown. The shape of the curve in the $|\dot{\mathbf{v}}|$-$|\dot{\omega}|$ plane indicates that linear and angular isotropic accelerations are nearly decoupled at the wrist point; i.e. Λ is nearly block diagonal.

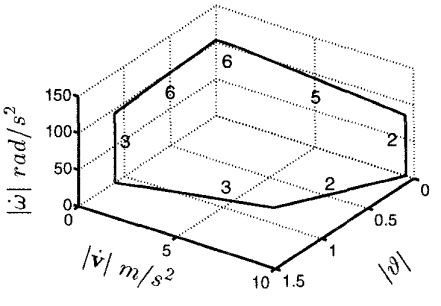

Figure 10

If the two accelerations were completely decoupled the curve would form a rectangle with the two coordinate axes. The same behavior is apparent in the $|\dot{\omega}|$-$|\vartheta|$ plane. The condition numbers of $E_{\mathbf{v}}$ and E_ω for this configuration are, $\kappa(E_{\mathbf{v}}) = 2.8$ and $\kappa(E_\omega) = 1.1$.

Figure 11 shows the isotropicity information for a different operational point about 6 inches out from

the wrist point at the same configuration as in Figure 10. The shape of the curves show much more coupling between each of the elements. The condition numbers for this configuration are $\kappa(E_{\mathbf{v}}) = 2.8$ and $\kappa(E_{\omega}) = 2.1$. Figure 12 shows the operational point of Figure 11 for a poorly conditioned configuration. Note the decrease in magnitudes of the isotropic accelerations. The condition numbers for this configuration are $\kappa(E_{\mathbf{v}}) = 54$ and $\kappa(E_{\omega}) = 26$.

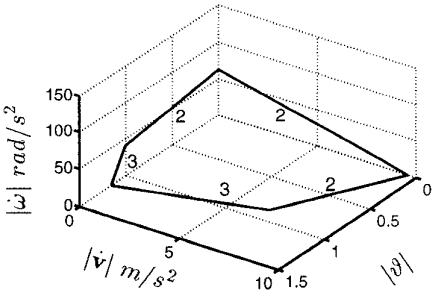

Figure 11

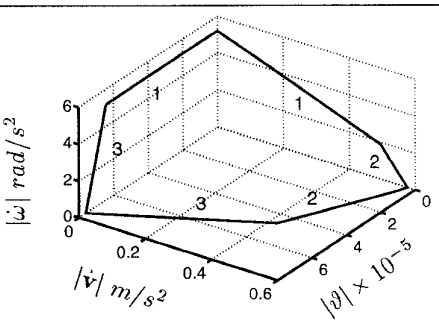

Figure 12

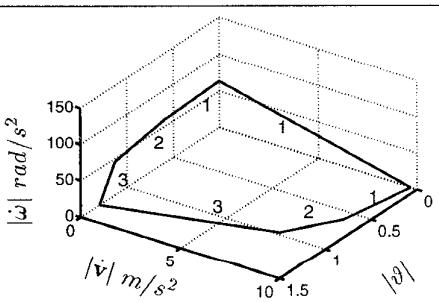

Figure 13

Finally, Figure 13 shows information for the same operational point and configuration as in Figure 11 with the maximum torques on joints 2 and 3 increased by 15% (in Figure 11 actuators 2 and 3 limit the isotropic accelerations). As compared to Figure 11, note the small increase in the isotropic acceleration and the much larger sustainable end-effector velocity before the point at which the isotropic acceleration is driven to zero.

Also notice that joint 1 has become the limiting actuator in the $|\dot{\mathbf{v}}|$-$|\dot{\omega}|$ plane which explains the small increase in the accelerations for that plane. Next one would try also to increase joint 1 actuator torque. It is also interesting to note that increasing the torques worsened the condition numbers; $\kappa(E_{\mathbf{v}}) = 3.1$ and $\kappa(E_{\omega}) = 2.1$.

5 Conclusion

We have presented an approach based on the *ellipsoid expansion* model for the analysis of linear and angular accelerations, given the limits on actuator torque capacities, at a given configuration. This model has been shown to provide a simple geometric solution for determining these accelerations. The result of the analysis is a surface which completely describes the dependency between the isotropic accelerations associated with linear and angular motions and end effector velocities. Condition numbers have been used to provide a measure of the extent of magnitude variations for the linear and angular accelerations in different directions. The results obtained with the PUMA 560 manipulator, illustrate the effectiveness of this approach for acceleration analysis. This approach is being extended to redundant manipulators.

6 Acknowledgments

The financial support of NASA/JPL, Boeing, Hitachi Construction Machinery, and NSF, grant IRI-9320017, are gratefully acknowledged. Many thanks to Michel Bilello who has made valuable contributions to this work.

References

[1] Yoshikawa T.; *Dynamic Manipulability of Robot Manipulators*, Proc. 1985 IEEE International Conference on Robotics and Automation, St. Louis, 1985, pp. 1033-1038.

[2] Khatib, O. and Burdick, J.; *Dynamic Optimization in Manipulator Design: The Operational Space Formulation*, The International Journal of Robotics and Automation, vol.2, no.2, 1987, pp. 90-98.

[3] Armstrong, B., Khatib, O., and Burdick, J.; *The Explicit Model and Inertial Parameters of the PUMA 560 Arm*, Proceedings IEEE Intl. Conference on Robotics and Automation, vol.1, pp. 510-518, 1986.